Tunable current partition at zero-line intersection of quantum anomalous Hall topologies

Yafei Ren,[1,2,3] Junjie Zeng,[2,3] Ke Wang,[2,3] Fuming Xu,[1,*] and Zhenhua Qiao[2,3,†]

[1]*Shenzhen Key Laboratory of Advanced Thin Films and Applications, College of Physics and Energy,*
Shenzhen University, Shenzhen 518060, China
[2]*ICQD, Hefei National Laboratory for Physical Sciences at Microscale, and Synergetic Innovation Center of Quantum Information and*
Quantum Physics, University of Science and Technology of China, Hefei, Anhui 230026, China
[3]*CAS Key Laboratory of Strongly-Coupled Quantum Matter Physics and Department of Physics,*
University of Science and Technology of China, Hefei, Anhui 230026, China

At the interface between two-dimensional materials with different topologies, topologically protected one-dimensional states (also named zero-line modes) arise. Here, we focus on the quantum anomalous Hall-effect-based zero-line modes formed at the interface between regimes with different Chern numbers. We find that these zero-line modes are chiral and unilaterally conductive due to the breaking of time-reversal invariance. For a beam splitter consisting of two intersecting zero lines, the chirality ensures that a current can only be injected from two of the four terminals. Our numerical results further show that, in the absence of contact resistance, the (anti-)clockwise partitions of the currents from these two terminals are the same owing to the current conservation, which effectively simplifies the partition laws. We find that the partition is robust against the relative shift of Fermi energy but can be adjusted effectively by tuning the relative magnetization strengths at different regimes or relative angles between zero lines.

I. INTRODUCTION

The presence of edge states that are topologically protected from backscattering is one of the striking hallmarks of topologically nontrivial insulators [1–5]. According to the rigorous bulk-edge correspondence rule [6,7], edge states appear at the boundary of two-dimensional topological systems, such as quantum Hall effect [8], quantum anomalous Hall effect [9,10], and quantum spin-Hall effect (or two-dimensional topological insulators) [11,12]. These edge states are localized at the boundaries that are interfaces between topological materials and topologically trivial vacuum. Thus, these boundaries can be generalized to interfaces between two topologically distinct materials, such as the interface between quantum anomalous Hall effect and quantum valley Hall effect [13], quantum spin-Hall effect and quantum valley Hall effect [14], or the graphene nanoroad between two structurally different boron nitride sheets [15]. One widely explored system is the zero-line modes (ZLMs) occurring at the interface across which the valley Chern number varies [1,16]. These ZLMs are protected from the long-range scattering potential by large momentum separation and exhibit zero bend resistance in the absence of atomic defects [15,17]. Such modes are experimentally feasible [18–20] in Bernal stacked multilayer graphenes with out-of-plane electric fields [21–23] and have attracted much attention from both theoreticians [1,17,24–35] and experimentalists [18–20,36].

Comparing to the sample boundary, the interface exhibits higher tunability, e.g., one can construct few interfaces as well as intersections to form networks [37,38]. At the intersection between zero lines of the quantum valley Hall effect, counterintuitive current partition was reported [37],

and later the tunable current partition at multiple intersections also was demonstrated [38]. In these systems, time-reversal invariance guarantees the helical transport of these ZLMs. In contrast, ZLMs based on the quantum anomalous Hall effect are chiral owing to the time-reversal-symmetry breaking and are topologically protected from backscattering even in the presence of short-range atomic scatters, suggesting more interesting transport properties.

In this article, we study the ZLMs formed at the interfaces between quantum anomalous Hall phases with opposite Chern numbers in graphene systems. We find that topologically protected ZLMs occur at both zigzag and armchair interfaces whereas the chiral edge states also appear at sample boundaries. These ZLMs are chiral and exhibit unilateral conductivity due to the breaking of time-reversal invariance, which are completely different from the ZLMs based on the quantum valley Hall effect. For a four-terminal setup composed of two intersected zero lines, the chirality of these modes ensures that the current can only be injected from two of the four terminals. Further numerical calculations show that the (anti-)clockwise partitions of the currents from these two different terminals are the same guaranteed by the current conservation in the absence of contact resistance. We then study the manipulation of current partition by external means and find that, different from the ZLMs based on the quantum valley Hall effect, the partition is robust against the relative shift of Fermi energy but can be tuned effectively by changing the relative magnetization strengths in different regions or the relative angles between neighboring terminals.

II. MODEL HAMILTONIAN AND BAND STRUCTURES

We employ the π-orbital tight-binding Hamiltonian of monolayer graphene with fixed Rashba spin-orbit coupling
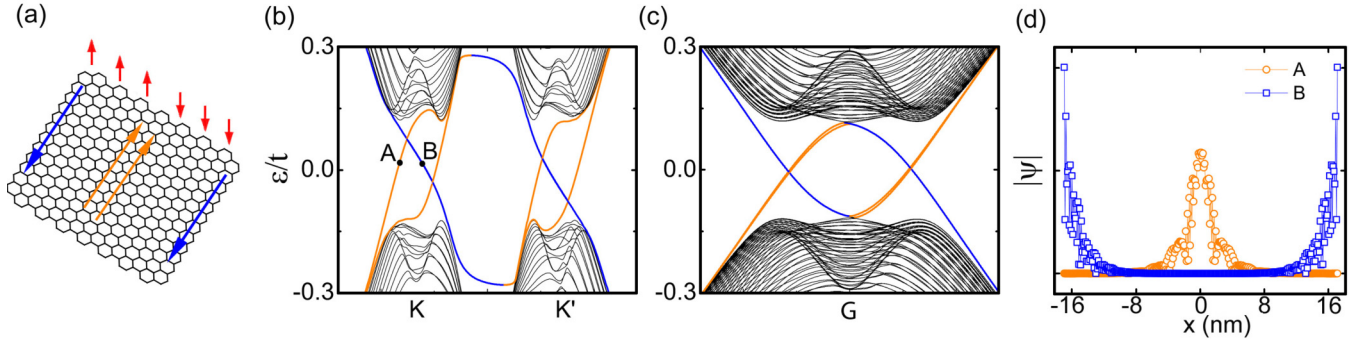
---

*xufuming@szu.edu.cn
†qiao@ustc.edu.cn

FIG. 1. (a) Schematic of ZLMs from different quantum anomalous Hall topologies. The left (right) side of the sample experiences an upward (downward) exchange field as shown by the red arrows. The orange arrows in the middle indicate the ZLMs, whereas the blue ones at the boundaries are edge states. (b) and (c) Band structures of zigzag- and armchair-terminated graphene nanoribbons with Rashba SOC $t_R/t = 0.10$. The orange and blue bands, respectively, are the ZLMs and edge modes. (d) Normalized probability amplitudes of wave functions for states "A" and "B" labeled in panel (b).

(SOC) and spatially varying out-of-plane magnetization, which can be expressed as [9]

$$H = -t \sum_{\langle ij \rangle} c_i^\dagger c_j + i t_R \sum_{\langle ij \rangle} c_i^\dagger (s \times \hat{d}_{ij}) \cdot \hat{z} \, c_j$$
$$+ \sum_i M_i f_i c_i^\dagger s_z c_i, \tag{1}$$

where $c_i^\dagger = (c_{i\uparrow}^\dagger, c_{i\downarrow}^\dagger)$ is the creation operator for an electron at the ith site with $\uparrow$ and $\downarrow$ representing the spin-up and spin-down states. The first term stands for the nearest-neighbor hopping with an amplitude of t, and the second term is the Rashba SOC involving only the nearest-neighbor hopping, where $\hat{d}_{ij}$ is a unit vector pointing from site j to i and the s's are spin-Pauli matrices. It is noteworthy that the strength of Rashba SOC shows a weak influence on the qualitative transport properties of ZLMs and its strength is set to be $t_R = 0.1t$ in our calculations without loss of generality. The third term represents the spatially varying out-of-plane exchange field where M_i measures its strength and $f_i = \pm 1$ indicates the upward (downward) orientation of the exchange field at site i.

In the presence of a uniform exchange field, Rashba SOC can induce a topologically nontrivial bulk band gap in monolayer graphene, hosting a quantum anomalous Hall state of Chern number ± 2 depending on the magnetization orientation [9]. When the exchange field varies spatially as shown by the red arrows in Fig. 1(a), quantum anomalous Hall topologies of Chern numbers $\mathcal{C} = \pm 2$ change between the left and the right sides, separately. Along the interface, unilaterally propagated ZLMs present as schematically plotted by orange arrows. The corresponding band structures of the zigzag and armchair graphene ribbons experiencing varying exchange fields are displayed in Figs. 1(b) and 1(c), respectively. The four nondegenerate orange bands are gapless ZLMs localized at the interface, whereas the blue bands are doubly degenerate edge modes, and there are two modes at each boundary as shown in Fig. 1(d). These states will be robust against weak disorders since the counterpropagating channels are separated spatially.

These ZLMs based on the quantum anomalous Hall effect exhibit some different characters from that based on the quantum valley Hall effect [17]. On one hand, for armchair nanoribbons in the latter case, edge states disappear, and ZLMs possess a small topologically trivial band gap due to the strong coupling between valleys K and K'. Here, however, both edge states and ZLMs appear for armchair nanoribbons and show rigorous gapless characters due to the topological protection, which makes it possible to investigate the transport properties at the charge neutrality point. On the other hand, different from the quantum valley Hall systems where the ZLMs at K and K' valleys show opposite group velocities guaranteed by the time-reversal invariance, such invariance is broken in quantum anomalous Hall systems, and the corresponding ZLMs propagate in the same direction for both valleys, whereas the edge states at the boundaries propagate along the opposite directions, resulting in the unilateral propagation of the ZLMs.

III. CURRENT PARTITION AT TOPOLOGICAL INTERSECTIONS

We now focus on the current partition at a four-terminal device composed of two intersecting zero lines as illustrated in Fig. 2 where ZLMs appear at the interface between regimes of $\pm\mathcal{C}$ with four terminals connecting to four leads labeled as up (U), down (D), left (L), and right (R). The current partition properties are obtained by studying the conductances among these four leads. In our calculation, the zero lines connecting U and D are set to be straight, whereas those connecting L and R are tunable by angles of α (between L and D) and β (between R and U) as shown in Fig. 2.

Our electronic transport calculations are based on the Landauer-Büttiker formalism [39] and recursively constructed Green's functions [40,41]. The conductance from terminal q to p is evaluated numerically by using $G_{pq} = (e^2/h)\text{Tr}[\Gamma_p G^R \Gamma_q G^A]$, where e is the electron charge, h is Planck's constant, $G^{R,A}$ are the retarded and advanced Green's functions of the central scattering regime, and Γ_p is a linewidth function describing the coupling between terminal p and the central region [40]. The current incoming from terminal p and its partition to other terminals can be illustrated schematically by plotting its contribution to the local density of states at energy ε: $\rho_p(\mathbf{r}, \varepsilon) = 1/2\pi[G^R \Gamma_p G^A]_{\mathbf{rr}}$, where $\mathbf{r}$ is the real-space coordinate. Without loss of generality, we set $\beta = 90°$ in the following calculations.
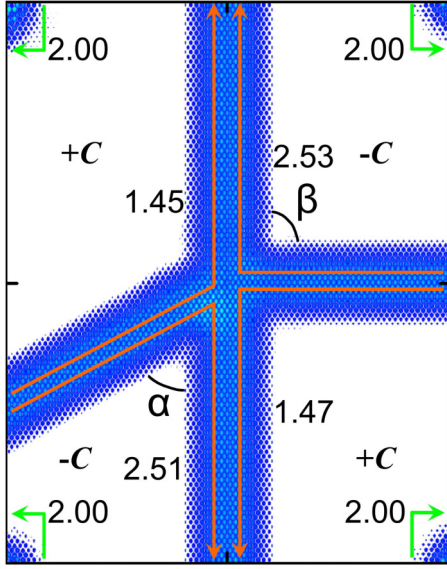
FIG. 2. Fermi-level scattering state density distributions in a four-probe zero-line intersection for zero-line configuration of $\alpha = 60°$ and $\beta = 90°$. The L, R, U, and D reservoirs each has a single zero line at the ribbon center which matches a system zero line at its boundary. Each point in these plots corresponds to an individual carbon atom site. The orange arrows in the middle indicate the currents flow along zero lines, whereas the green ones at the corners suggest the currents flow along the edges. The number near each orange arrow represents the currents partitioned into U or D terminals from L or R. $G_{\mathrm{UL,DL}}$ are not exactly the same as $G_{\mathrm{DR,UR}}$ due to the finite-size effect of the left lead. $\pm\mathcal{C} = \pm 2$ stands for the Chern number at each regime.

A. Unilateral transport and partition laws of ZLMs

Due to the chirality of these ZLMs, one may naturally expect such a four-terminal device will exhibit unilateral conductivity similar to a p-n junction, i.e., given the configuration of magnetization orientations, the current can only be injected into the zero lines from two terminals but be output via another two as illustrated in Fig. 2 where the current density is denoted in color and the current can only flow from L/R to U/D terminals along the zero lines as suggested by the orange arrows. The number near each orange arrow labels the conductance of that channel. One can find that more portions of the current from terminal L are partitioned into terminal D when the angle between L and D is smaller than that between L and U, similar to the counterintuitive partition law in the quantum valley Hall-effect-based zero-line intersection [37]. For the U/D terminal, however, the current can only be injected through the edge states with quantized conductances as suggested by the green arrows. We summarize the transport rules from the numerical calculations in the following:

$$G_{\mathrm{RL}} = G_{\mathrm{LR}} = G_{\mathrm{UD}} = G_{\mathrm{DU}} = 0.00 e^2/h, \quad (2)$$

$$G_{\mathrm{UL}} + G_{\mathrm{DL}} = G_{\mathrm{UR}} + G_{\mathrm{DR}} = 4.00 e^2/h, \quad (3)$$

$$G_{\mathrm{RU}} = G_{\mathrm{LU}} = G_{\mathrm{RD}} = G_{\mathrm{LD}} = 2.00 e^2/h, \quad (4)$$

$$G_{\mathrm{UL}} = G_{\mathrm{DR}}, \quad (5)$$

$$G_{\mathrm{DL}} = G_{\mathrm{UR}}. \quad (6)$$

Equation (2) reflects the forbidden forward transmission due to the chirality of ZLMs. Along zero lines, the current is injected from L or R and is partitioned into U and D terminals, giving rise to finite but unnecessarily quantized values of $G_{\mathrm{U/D,L}}$ and $G_{\mathrm{U/D,R}}$. The current conservation leads to the fact that the sum of partitioned currents to U and D terminals equals the incident current from L or R as shown in Eq. (3). As for the current from U or D to L and R terminals, they can only propagate along the sample boundaries, and quantized conductances appear as reflected by Eq. (4). These quantized values are very robust against the variation of α/β, Fermi energy, etc., because the edge modes are not mixed with other states (either ZLMs or other edge modes) for a large enough sample. It is noteworthy that these quantized values G_{pq} are generally different from G_{qp} as they transport along different paths. This is different from the current partition rules at the zero-line intersections based on the quantum valley Hall effect where the edges do not contribute to conductance and $G_{qp} = G_{pq}$ always is guaranteed by the time-reversal invariance [37].

Moreover, our numerical results also suggest that the clockwise (anticlockwise) partition of currents injected from the L or R terminal are the same as indicated in Eqs. (5) and (6), i.e., current from the L to the U (D) terminal is the same as that from R to D (U). It is noteworthy that, in Fig. 2, $G_{\mathrm{UL,DL}}$ are not exactly the same as $G_{\mathrm{DR,UR}}$ due to the finite-size effect of the left lead. Such a feature effectively simplifies the current partition laws in such four-terminal devices, making it possible to be characterized by only one parameter. These results are similar to the current partition laws in the quantum valley Hall-effect-based zero-line intersection [37], which are originated from the current conservation and the relation of $G_{pq} = G_{qp}$ guaranteed by time-reversal invariance. However, as mentioned above, the breaking of time-reversal invariance in the quantum anomalous Hall system invalidates the relationship of $G_{pq} = G_{qp}$. What is the physical origin of relations shown in Eqs. (5) and (6)?

This can be attributed to the current conservation and the absence of contact resistance. In general, we can describe the partition of current from L or R by two separate parameters, i.e., the current partition for terminal L is G_{UL} and $(4 - G_{\mathrm{UL}})$, whereas that for terminal R is G_{UR} and $(4 - G_{\mathrm{UR}})$. One can consider the case of injecting currents from L and R simultaneously. In the absence of contact resistance, each of the L and R terminals can inject a current of $\delta_V 4e^2/h$ giving rise to a total current of $\delta_V 8e^2/h$ with δ_V being the voltage difference between L/R and U/D terminals. These currents will be output into both U and D terminals. Since both U and D can only support no more than a $\delta_V 4e^2/h$ current, each terminal can and has to carry $\delta_V 4e^2/h$. As a result, the current partition from R to U must be the same as that from L to D, i.e., $G_{\mathrm{UR}} = 4 - G_{\mathrm{UL}} = G_{\mathrm{DL}}$. The case is similar for G_{DR} and G_{UL}. Such a simple analysis can be generalized to cases when the absolute values of the Chern numbers at different regimes are unequal. It is noteworthy that the above analysis is based on the assumption that there is no contact resistance between the central scattering regime and the terminals. In the presence of such resistance induced by disorder, lattice mismatch, or spin polarization in leads, the partition laws in Eqs. (5) and (6) are no longer exactly valid.
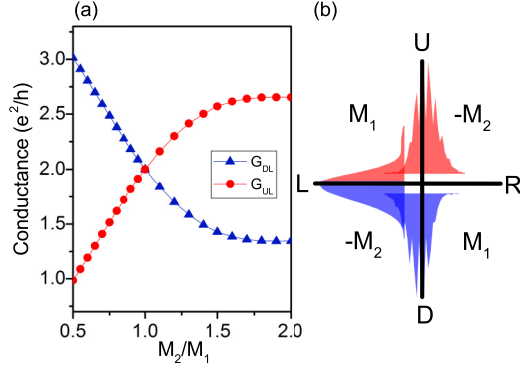
FIG. 3. (a) Conductances G_{UL} and G_{DL} vs relative exchange field strength M_2/M_1 at a fixed structure with $\alpha = 90°$ at the charge neutrality point. (b) Schematic of the probability amplitudes of ZLMs at different zero lines with $M_2/M_1 = 0.5$. Here, we set $M_1 = 0.2t$. More overlaps between ZLMs on L and D appear.

B. Tuning current partition via magnetization

We fix the system structures by setting $\alpha = \beta = 90°$ to investigate the role of relative exchange field strengths between neighboring quadrants. The Rashba SOC strength is fixed at $t_R = 0.1t$. We denote the exchange fields in the top-left, top-right, bottom-left, and bottom-right quadrants as $(+M_1, -M_2, -M_2, +M_1)$ with $M_1 = 0.2t$ here and $\pm$ indicating upward or downward orientation. By changing the magnitude of M_2, one can investigate the dependence of the current partition on M_2/M_1 as shown in Fig. 3. One can find that the half-half current partition appears at $M_2 = M_1$. When $M_2 < M_1$, one can find that more current from L is partitioned into D. When $M_2 > M_1$, the trend of the current partition becomes opposite. Thus, one can conclude that the current prefers to flow around the region with smaller magnetization.

Such findings can be understood from the dependence of the wave functions of ZLMs on magnetization M. In a graphene system, the presence of out-of-plane magnetization splits the spin degeneracy of energy bands and leads to band crossing around the Dirac points. The further introduction of Rashba SOC lifts the degeneracies of band crossings to form band gaps harboring the quantum anomalous Hall effect [9]. For relatively small Rashba SOCs, the band gap is proportional to the strength of the Rashba SOC, which shows nearly linear dependence on momentum. Therefore, as the magnetization strength increases, a larger band gap is expected. Generally, a larger band gap indicates a stronger topological confinement leading to smaller wave-function extension. As shown in Fig. 3(b), the wave functions of ZLMs are more extended in the bottom left and top-right regimes where the magnetization strength is smaller. As a result, at the zero-line intersection, the wave functions of the ZLMs on L show more overlap with that on D leading to a larger current partition from L to D.

C. Tuning the current partition via the angle of incidence

We then study the current partition for different α's at fixed $\beta = 90°$. By setting the Fermi energy to be zero, we calculate the conductances between different terminals and plot G_{UL} and G_{DL} as a function of $\alpha + \beta$ in Fig. 4(a). One can find that the current partition exhibits strong dependence
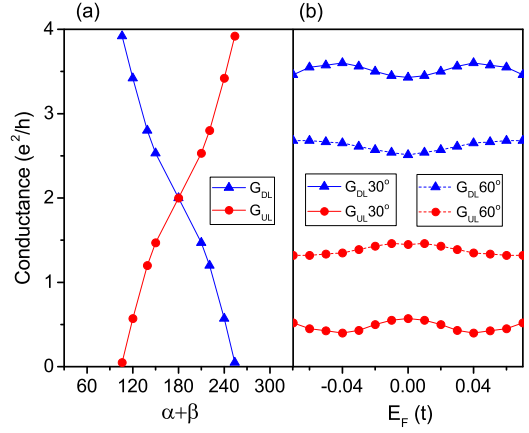

FIG. 4. (a) Conductances G_{UL} and G_{DL} vs $\alpha + \beta$ at the charge neutrality point $E_F = 0$ with $\beta = 90°$. (b) G_{UL} and G_{DL} vs Fermi energy E_F for a fixed structure with $\beta = 90°$ and $\alpha = 30°$ or $60°$.

on α. To be specific, when $\alpha < 16.1°$, the left zero line is much closer to the down one, and thus the ZLMs along these two zero lines show larger spatial overlap, making almost all the currents be partitioned from L to D. As α increases, the currents partitioned to U gradually increase, and the equal current partition occurs at $\alpha = 90°$ that corresponds to a highly symmetric structure. It is noteworthy that when $\beta \neq 90°$, the condition of equal partition can be generalized to be $\alpha + \beta = 180°$. In this case, the system is invariant under mirror reflection about the vertical zero line, which guarantees $G_{DL} = G_{DR}$. By combining with Eq. (5), one can find that $G_{DL} = G_{UL}$. As α further increases, more currents are partitioned into U. These behaviors are qualitatively similar to that of a zero-line intersection based on the quantum valley Hall effect reported in Ref. [37] whereas quantitatively different as the dependence of the current partition on $\alpha + \beta$ deviates from the sinusoidal function.

D. Tuning the current partition via the Fermi energy

Here, we explore the influence of Fermi energy at fixed structures with $\alpha = 30°$ or $60°$ as displayed in Fig. 4(b) with the solid and dashed lines, respectively. One can find that, different from the strong dependence on the angle of incidence α, the current partition is quite robust against the Fermi energy. The relative variation of G_{UL} (G_{DL}) is around 10% when the Fermi level approaches the conduction-band minimal or valence-band maximal. Such dependence of the current partition on the Fermi energy is completely distinct from that in the zero-line intersection based on the quantum valley Hall effect. On one hand, the system is gapped at the charge neutrality point for the latter case as the armchair boundary involves. On the other hand, the partition of the current rapidly becomes equal as the Fermi energy approaches the band extrema [37].

IV. SUMMARY

We have numerically studied the electronic structures and wave functions of ZLMs from spatially varying quantum

anomalous Hall topologies. Both ZLMs and edge states exhibit gapless characters due to topological protection. The breaking of time-reversal invariance leads to unilaterally propagating ZLMs. At the intersection of such zero lines, we have further investigated the partition laws of the current flowing along zero lines. The chirality of the quantum anomalous Hall effect makes the current along zero lines only be injected from two of the four terminals (e.g., L and R) and be output from the other two (e.g., U and D). In the absence of contact resistance, even though the time-reversal invariance is breaking, the current conservation guarantees the equivalence between the clockwise partitions of currents from the L and R terminals, which greatly simplifies the current partition law to be determined by only one parameter. Different from the quantum valley Hall-based topological intersection, the current partition is robust against the variation of Fermi energy. We further show that the current partition is externally tunable. By changing the relative angles between different zero lines, we find that the partition of the current prefers a sharp turn. Moreover, the current partition can also be tuned effectively by changing the relative magnetization strengths at different regions, and the current prefers to flow around the regions with lower magnetization strength. Such a tunability indicates

potential applications in low-energy consumption electronics. By making use of this current splitter, we can obtain a tunable current propagating from the L/R to the U/D terminals along zero lines and a robust current propagating from the U/D to the L/R terminals along the edges. In this way, one can fabricate electronics which can produce both tunable and constant current streams. Experimentally, the quantum anomalous Hall effect is proposed to appear in graphene with an insulating (anti-)ferromagnetic substrate [42]. Thus, the ZLMs and their intersections from quantum anomalous Hall topologies naturally are expected at the domain walls of the magnetic substrate.

[1] Y. Ren, Z. Qiao, and Q. Niu, Rep. Prog. Phys. **79**, 066501 (2016).

[2] M. Z. Hasan and C. L. Kane, Rev. Mod. Phys. **82**, 3045 (2010).

[3] X. Qi and S. Zhang, Rev. Mod. Phys. **83**, 1057 (2011).

[4] K. He, X. C. Ma, X. Chen, L. Lü, Y. Y. Wang, and Q. X. Xue, Chin. Phys. B **22**, 067305 (2013).

[5] A. Bansil, H. Lin, and T. Das, Rev. Mod. Phys. **88**, 021004 (2016).

[6] Y. Hatsugai, Phys. Rev. Lett. **71**, 3697 (1993).

[7] G. M. Graf and M. Porta, Commun. Math. Phys. **324**, 851 (2013).

[8] K. von Klitzing, Séminaire Poincaré **2**, 1 (2004).

[9] Z. Qiao, S. A. Yang, W. Feng, W. K. Tse, J. Ding, Y. Yao, J. Wang, and Q. Niu, Phys. Rev. B **82**, 161414(R) (2010).

[10] R. Yu, W. Zhang, H. J. Zhang, S. C. Zhang, X. Dai, and Z. Fang, Science **329**, 61 (2010).

[11] D. N. Sheng, Z. Y. Weng, L. Sheng, and F. D. M. Haldane, Phys. Rev. Lett. **97**, 036808 (2006).

[12] B. A. Bernevig, T. L. Hughes, and S. C. Zhang, Science **314**, 1757 (2006).

[13] H. Pan, X. Li, F. Zhang, and S. A. Yang, Phys. Rev. B **92**, 041404(R) (2015).

[14] M. Wang, L. Liu, C.-C. Liu, and Y. Yao, Phys. Rev. B **93**, 155412 (2016).

[15] J. Jung, Z. Qiao, Q. Niu, and A. H. MacDonald, Nano Lett. **12**, 2936 (2012).

[16] I. Martin, Y. M. Blanter, and A. F. Morpurgo, Phys. Rev. Lett. **100**, 036804 (2008).

[17] Z. Qiao, J. Jung, Q. Niu, and A. H. MacDonald, Nano Lett. **11**, 3453 (2011).

[18] L. Ju, Z. Shi, N. Nair, Y. Lv, C. Jin, J. Velasco, Jr., C. Ojeda-Aristizabal, H. A. Bechtel, M. C. Martin, A. Zettl, J. Analytis, and F. Wang, Nature (London) **520**, 650 (2015).

[19] J. Li, K. Wang, K. J. McFaul, Z. Zern, Y. F. Ren, K. Watanabe, T. Taniguchi, Z. H. Qiao, and J. Zhu, Nat. Nanotechnol. **11**, 1060 (2016).

[20] J. Li, R.-X. Zhang, Z. Yin, J. Zhang, K. Watanabe, T. Taniguchi, C. Liu, and J. Zhu, arXiv:1708.02311 (2017).

[21] D. Xiao, W. Yao, and Q. Niu, Phys. Rev. Lett. **99**, 236809 (2007).

[22] Z. Qiao, W. K. Tse, H. Jiang, Y. Yao, and Q. Niu, Phys. Rev. Lett. **107**, 256801 (2011).

[23] X. Li, Z. Qiao, J. Jung, and Q. Niu, Phys. Rev. B **85**, 201404 (2012).

[24] J. R. Anglin and A. Schulz, Phys. Rev. B **95**, 045430 (2017).

[25] J. Jung, F. Zhang, Z. Qiao, and A. H. MacDonald, Phys. Rev. B **84**, 075418 (2011).

[26] F. Zhang, A. H. MacDonald, and E. J. Mele, Proc. Natl. Acad. Sci. USA **110**, 10546 (2013).

[27] J. Li, A. F. Morpurgo, M. Büttiker, and I. Martin, Phys. Rev. B **82**, 245404 (2010).

[28] J. Li, I. Martin, M. Büttiker, and A. F. Morpurgo, Phys. Scr. **T146**, 014021 (2012).

[29] G. W. Semenoff, V. Semenoff, and F. Zhou, Phys. Rev. Lett. **101**, 087204 (2008).

[30] W. Yao, S. A. Yang, and Q. Niu, Phys. Rev. Lett. **102**, 096801 (2009).

[31] S. K. Wang, J. Wang, and K. S. Chan, New J. Phys. **16**, 045015 (2014).

[32] A. Vaezi, Y. Liang, D. H. Ngai, L. Yang, and E. A. Kim, Phys. Rev. X **3**, 021018 (2013).

[33] Y. Kim, K. Choi, J. Ihm, and H. Jin, Phys. Rev. B **89**, 085429 (2014).

[34] M. Kindermann, B. Uchoa, and D. L. Miller, Phys. Rev. B **86**, 115415 (2012).

[35] J. Song, H. Liu, H. Jiang, Q. F. Sun, and X. C. Xie, Phys. Rev. B **86**, 085437 (2012).

[36] J. S. Alden, A. W. Tsen, P. Y. Huang, R. Hovden, L. Brown, J. Park, D. A. Muller, and P. L. McEuen, Proc. Natl. Acad. Sci. USA **110**, 11256 (2013).

[37] Z. Qiao, J. Jung, C. Lin, Y. Ren, A. H. MacDonald, and Q. Niu, Phys. Rev. Lett. **112**, 206601 (2014).

[38] K. Wang, Y. Ren, X. Deng, S. A. Yang, J. Jung, and Z. Qiao, Phys. Rev. B **95**, 245420 (2017).

[39] S. Datta, *Electronic Transport in Mesoscopic Systems* (Cambridge University Press, Cambridge, UK, 1995).

[40] M. P. Lopez Sancho, J. M. Lopez Sancho, and J. Rubio, J. Phys. F **14**, 1205 (1984).

[41] J. Wang and H. Guo, Phys. Rev. B **79**, 045119 (2009).

[42] Z. Qiao, W. Ren, H. Chen, L. Bellaiche, Z. Zhang, A. H. MacDonald, and Q. Niu, Phys. Rev. Lett. **112**, 116404 (2014).